www.lajss.org
Latin American Journal of Solids and Structures 3 (2006) 361–376

Measurement of the ratio G_F/G_f for numerical analysis of concrete structures

R. A. Einsfeld[1,*] and M. S. L. Velasco[2]

[1] Polytechnic Institute (IPRJ), State University of Rio de Janeiro (UERJ), RJ – Brazil
[2] Department of Civil Engineering, Pontifical Catholic University of Rio de Janeiro (PUC-Rio), RJ – Brazil

Abstract

The fracture energies G_F, obtained by the work-of-fracture method, and G_f, obtained by the size effect method, are two different material characteristics. The fracture energy G_F represents the area under the complete load-deflection curve, and the fracture energy G_f represents the area under the initial tangent of the softening curve. It is possible to show through numerical simulation of notched fracture specimens that, at maximum load, the cohesive crack will never be opened enough for the tail stresses of the softening curve to occur. Consequently, G_f determines the maximum load of most concrete structures in practice. Nevertheless, many finite element programs request the complete softening curve corresponding to the fracture energy G_F. In this case, the ratio G_F/G_f is worthy to be investigated because the energy G_f is easier to be obtained through the experiments. In this work, the correlation between G_F and G_f is investigated. The results obtained in an experimental program, developed at PUC-Rio in order to study the fracture properties of high-performance concrete, are presented and compared with some results showed in the literature. A numerical example illustrates the development of the cohesive zone during specimen testing.

Keywords: fracture energy, fracture mechanics of concrete, concrete structures, numerical analysis, experimental analysis

1 Introduction

The use of fracture mechanics in design can increase the safety and reliability of concrete structures, and it is no doubt especially important when these structures are manufactured with high-strength concrete. The most important aspect of its application is the possibility of incorporating in design practice the influence of the size of the structure in the structural strength, known as the size effect. Many analytical and numerical tools were developed to simulate the fracture behavior of concrete structures, and nowadays much research effort is devoted to develop experimental methods to measure the parameters entering the various numerical models.

*Corresp. author email: einsfeld@iprj.uerj.br Received 12 April 2006; In revised form 29 May 2006

The simplest model that describes the progressive fracture process is the cohesive crack model, which was proven useful in explaining most experimental results when testing concrete, as shown by Hillerborg et al. [21], Bazant et al. [5], Carpinteri [12] and many other researchers in this field.

The softening curve is the main feature of the cohesive crack model. This curve is characterized by an initial portion with a steep descending slope, followed by a smooth drop when the stress reaches a value approximately equal to 1/3 of the nominal tensile strength, and a long tail asymptotic to the horizontal axis, as shown in Figure (1). Geometrically, the area under the complete softening curve coincides with the fracture energy G_F. However, from numerical examples it is possible to observe that only the initial part of the softening curve is necessary to determine the peak load for normal-sized structures. Therefore, the entire softening curve can be replaced in the constitutive model by a straight line corresponding to the initial tangent of the softening stress-separation curve. The fracture energy that corresponds to the area under the initial tangent of the softening curve is denoted G_f.

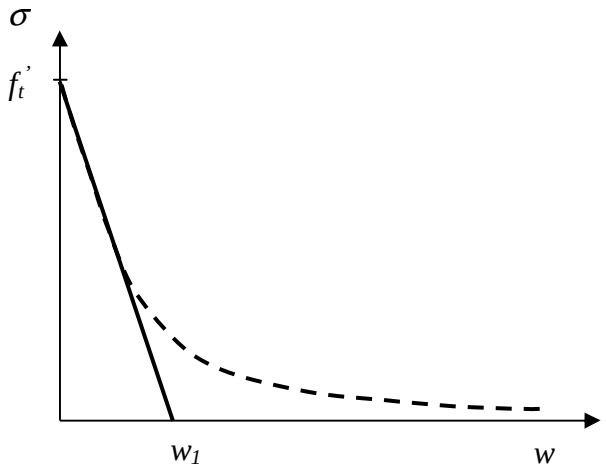

Figure 1: Softening function and initial tangent.

Most commercial programs that perform finite element analysis using cohesive crack models request the complete softening curve corresponding to the fracture energy G_F. Therefore, since the initial fracture energy G_f is easier to be determined experimentally, the ratio G_F/G_f is worthy to be investigated, allowing G_F to be estimated from G_f. In this work, the ratio G_F/G_f is obtained from experimental tests accomplished at PUC-Rio for High Performance Concrete (HPC) and the values are compared with the results obtained by Bazant and Becq-Giraudon [3, 4]. A numerical example is performed in order to show that the energy G_f suffices for predicting the limit load of most concrete structures.

2 The softening function

The cohesive crack model was developed to simulate the nonlinear material behavior at the concrete fracture process zone, where the crack is assumed to open and to extend while still able to transfer stress from one face to the other. The fracture process zone can be described by the discrete or the smeared approaches. In the discrete approach, as in Hillerborg's fictitious crack model [21], the concrete softening behavior is characterized by the tensile strength $f_t^{'}$ and the fracture energy G_F. In the smeared approach, as in the Bazant's crack band model [6], the cracks are supposed to be distributed in a certain region of the structure and a third parameter is necessary in order to characterize the material softening behavior, besides the two aforementioned. This parameter relates the fracturing strain into the cracked region to the crack opening w of the cohesive crack, and is considered as a material property. For mode I opening, the stress transferred is normal to the crack faces and is a unique function of the crack opening, i.e., $\sigma = f(w)$.

The softening curves are determined experimentally for different mixes of concrete and are similar in shape to the exponential curve represented in Figure (2) [8]. The curves shown in Figure (2) are plotted nondimensionally by dividing σ by $f_t^{'}$ and w by w_{ch}, where w_{ch} is equal to $G_F/f_t^{'}$. In numerical analysis, however, simplified softening functions for these curves are used, ranging from very simple to more sophisticated equations. Some of them are also represented in the figure. The simplest are the rectangular and linear softening curves, but both usually overestimate the strength of normal-sized structures. The bilinear and exponential curves provide better results when performing numerical analysis. The bilinear curve was initially proposed by Petersson [22], followed by other curves almost coincident but with some differences regarding the size of the tail and the location of the kink point (see for instance the works of Roelfstra and Wittmann [25] and Rokugo et al. [26]).

The bilinear softening function is probably the most required in numerical programs. In order to fit the experimental data, there are some methods proposed in the literature that adjust the position of the kink point and the length of the tail. The curves proposed by the CEB-FIP Model Code [14], for instance, depend on the maximum aggregate size of the concrete mix. Guinea et al. [19] give in their work explicit expressions for bilinear softening using the data relative to the stable fracture test and from the cylinder splitting test.

For not too large specimens, only the initial part of the softening curve is necessary to compute the peak load, as shown by Guinea et al. [18] and Bazant et al. [9]. The fracture energy corresponding to the area under the initial part of the softening curve is denoted as G_f. It corresponds to the energy required for crack growth in an infinitely large specimen.

The total fracture energy G_F is normally associated with the fictitious crack model and is obtained computing the total area under the load-deflection diagram divided by the area of the ligament. The values obtained by this method, called the work-of-fracture method (WFM), are sensitive to the size and shape of the specimens. The initial fracture energy G_f is obtained by the size effect method (SEM) and is independent of the size and the geometry of the specimens.

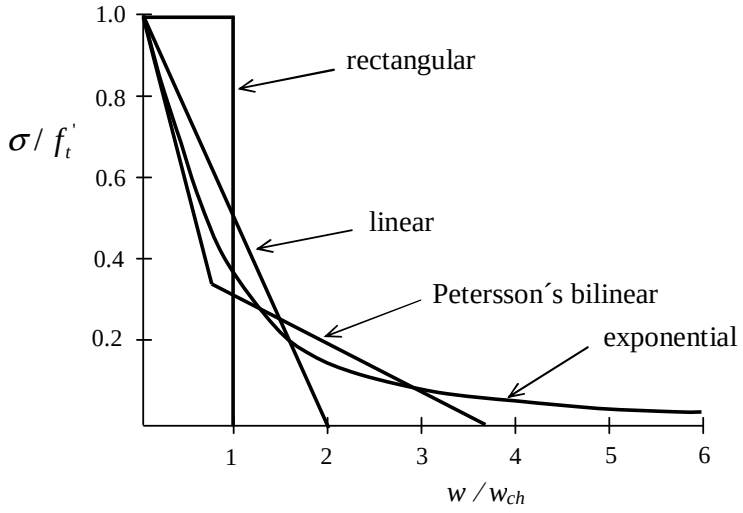

Figure 2: Analytical softening curves (adapted from Bazant and Planas [8]).

The softening stress-separation curve of cohesive crack model and areas representing the total fracture energy G_F and the initial fracture energyG_f are shown in Figure (3).

Through numerical simulation for normal-sized structures, it is possible to show that the maximum load of a specimen is reached when the cohesive stress is reduced to only 50% to 75% of $f_t^{'}$ [9]. Therefore, the cohesive crack will never be opened enough for the tail stresses of the softening curve to occur and, hence, the numerical model will provide the same maximum load if the cohesive model is replaced by a straight line corresponding to the initial tangent of the softening stress-separation curve. This greatly simplifies the problem, since the whole softening curve is not needed and the energy G_f is easier to be obtained through the experiments.

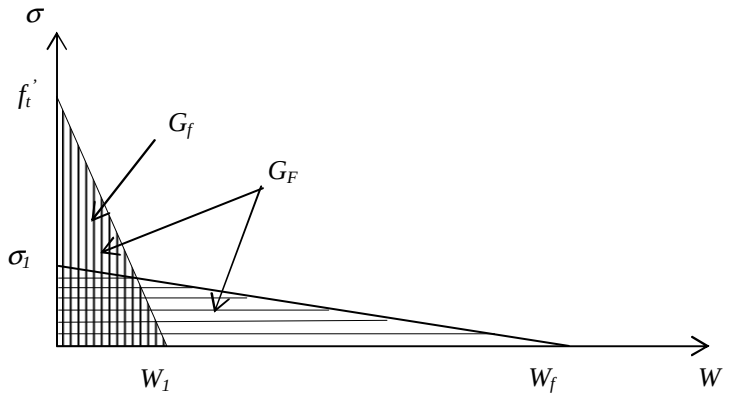

Figure 3: Softening stress-separation curve of cohesive crack model [9].

3 Determination of G_F and G_f

In order to determine the fracture energy G_F, one can apply the recommendation of the Technical Committee RILEM 50–FMC [1] to perform three-point bend tests in notched beams. The fracture energy is defined as the amount of energy necessary to create a crack of unit surface area projected in a plane parallel to the crack direction. As the beam is split in two halves, the fracture energy can be determined dividing the total dissipated energy by the total surface area of the crack:

$$G_F = \frac{W}{b(d - a_0)} \tag{1}$$

where W is the total energy dissipated in the test, b is the thickness, d is the height and a_0 is the notch depth of the beam.

This method, also known as work-of-fracture method (WFM) or Hillerborg's method [20], delivers fracture characteristics that are size-dependent. As a consequence, different values for the fracture energy are obtained for specimens of different sizes. In an alternative method proposed by Bazant and Pfeiffer [7], the fracture energy is determined from the size effect law. If geometrically similar beams are used and the load at rupture extrapolated to a beam of infinite dimensions, the fracture energy must have one single value, regardless the type, size or shape of the specimen. In this case, by definition, the value of the fracture energy is independent of the size of the specimens. This procedure is known as the size effect method (SEM).

Through this asymptotic approach, the problem is now reduced to finding and applying the correct law for the size effect. Bazant and Pfeiffer suggested the following relationship:

$$\sigma_N = B(1 + \beta^k)^{-\frac{1}{2k}} \tag{2}$$

where σ_N is the nominal stress at failure, B is a coefficient obtained through the linear regression plot of the test results, β is the brittleness number and k is a parameter which can be optimized for a most accurate representation of the size effect. Nevertheless, according to Bazant and Pfeiffer, no case was found in practice in which this optimization had been necessary, and usually the value of $k = 1$ is applied.

The nominal stress is obtained from the experimental tests as:

$$\sigma_N = C_n \frac{P_u}{bd} \tag{3}$$

where P_u is the ultimate load and C_n is a coefficient introduced for convenience.

The brittleness number indicates whether the behavior of any structure is related to limit state analysis or to linear elastic fracture mechanic (LEFM) analysis. Bazant and Pfeiffer propose the following equation for the brittleness number:

$$\beta = \frac{d}{d_0} \tag{4}$$

where d is the characteristic dimension of the structure (the specimen height in this study) and d_0 is a coefficient determined experimentally.

The value of β= 1 corresponds to the transition point between the strength approach and the LEFM approach. For values of $\beta \leq 0.1$, the plastic limit analysis should be used for structural design, and for values of $\beta \geq 10$, the LEFM should be used. For $0.1 < \beta < 10$, the nonlinear fracture mechanics should be used for structural design.

The coefficients B and d_0 in Equations (2) and (4), respectively, are determined by linear regression. For this purpose, Equation (2), applicable to geometrically similar specimens of different sizes, can be algebraically rearranged to a linear regression plot $Y = AX + C$, in which:

$$Y = (1/\sigma_N)^2; \quad X = d; \quad d_0 = C/A; \quad B = 1/\sqrt{C} \tag{5}$$

Rupture of a structure of infinite size follows the LEFM theory, since the plastic region around the concrete fracture zone is relatively small. In this case, the fracture energy G_f can be calculated as:

$$G_f = \frac{g_f(\alpha_0)}{AE} \tag{6}$$

where E is the Young's elastic modulus of the concrete, A is the angular coefficient of the linear regression plot, $g_f(\alpha_0)$ is the non-dimensional energy release rate calculated according to LEFM and found in many books as Reference [2], and α_0 is the relative notch length (a_0/d).

4 Experimental study

Three-point bend tests for geometrically similar notched specimens with four different sizes were used in order to determine the fracture energy through the SEM besides the WFM [11,27]. All tests were performed at the Technological Institute at PUC (ITUC) using closed-loop servo-controlled testing machines equipped with load cells of 25 kN and 50 kN capacity. The specimens had depths (d) of 38.1, 76.2, 152.4 and 304.8 mm, with the same thickness (b) of 38.1 mm, lengths equal to 2.67d, and spans equal to 2.5d, as shown in Figure (4). The results obtained for 67 specimens, classified in six Series of concrete batches (Series S1 to S6), are analyzed in this study. A more comprehensive analysis of the investigations conducted by the authors at PUC-Rio on the determinations of fracture parameters for high-performance concrete, including the results presented in this paper, can be seen in Reference [16].

Series S1 to S5 contain three specimens for each of the four heights. For Series S6, six specimens were molded for each beam height. The notch depth a_0 was equal to 1/3 of the height of the beams for the first two Series, and equal to 1/6 of the beam height for Series S3 to S6. For Series S1 to S5, the notch was precast with an acrylic plate with the thickness of 2 mm. For Series S6 the notches were saw-cut after curing.

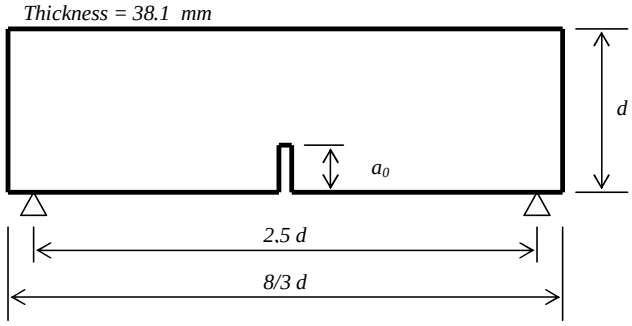

Figure 4: Geometric configuration for the specimens tested.

All the specimens were cast using high performance concrete (HPC), proportioned with a low water-to-cimentitious materials ratio and the inclusion of microssilica to the concrete mixture. The concrete mixes, labeled HP1, HP2 and HP3 in this work, were designed to exceed a 28-day compressive strength of 70, 90 and 110 MPa, respectively. Along with the beam specimens, six 100 x 200 mm cylinders were cast for each Series. The average 28-day values of the compressive stress were 84 MPa (±6.3%) for Series S1 (mix HP2), 82 MPa (±3.5%) for Series S2 (mix HP2), 78 MPa (±3.1%) for Series S3 (mix HP2), 69 MPa (±2.2%) for Series S4 (mix HP3), 78 MPa (±3.5%) for Series S5 (mix HP1) and 88 MPa (±2.0%) for Series S6 (mix HP2). The lower values achieved for the compressive strength in relation to the target compressive strength can be attributed to the type of aggregate (gneiss) used in the concrete mixes and its maximum size (9.5 mm). Differently from the normal-concrete, the compressive strength of high-strength concrete can be limited by the aggregate strength, as pointed by Darwin et al. [15], and by the size of the coarse aggregate, as shown in the work of Rao and Prasad [24].

For Series S1 and S2, the tests were controlled by the vertical displacement of the load cell. The results for the beams with height equal to 304.8 mm with deeper notches happened to be unstable under direct displacement control. For Series S3 to S6, all the specimens were tested under crack-mouth opening displacement (CMOD) control, which allowed the acquisition of load-CMOD and complete load-deflection curves for all specimen sizes. Table (1) shows the values obtained for the fracture energy G_F according to the work-of-fracture method.

The fracture energy obtained by the SEM, was computed as specified in RILEM TC89-FMT [28]. The nominal stresses, computed according to Equation (3) with C_n=1 and using the corrected maximum loads obtained from the tests, are shown in Table (2). The corrected maximum loads were obtained by adding half the beam self-weight to the measured peak load, in order to take the effect of the weight of the specimen into account for fracture energy determination. The values denoted with an asterisk are inconsistent with the trend of the other tests and were not considered for the determination of the fracture energy. Some beams were not tested due to the evidence of small flaws around the beam notch, which can be attributed to problems during the compaction and handling of the specimens.

Table 1: Values of average G_F measured for specimens tested in Series S1 to S6 (adapted from Reference [16]).

Series (Concrete)	f'_c (MPa)	a_0/d	Average G_F (N/m)			
			Depth d(mm)			
			38.1	76.2	152.4	304.8
S1 (HP2)	84	0.333	132	170	183	NM
S2 (HP2)	82	0.333	112	168	208	NM
S3 (HP2)	78	0.167	108	123	135	145
S4 (HP3)	69	0.167	121	127	146	168
S5 (HP1)	78	0.167	NT	127	144	150
S6 (HP2)	88	0.167	140	153	185	219

NT = specimens not tested NM = values not measured

Table 2: Nominal stresses obtained from peak loads of tested specimens.

Depth d (mm)	Nominal stress σ_N (MPa)						
	Series						
	S1	S2	S3	S4	S5	S6	
38.1	1.02	1.03	1.44	1.48	NT	1.41	1.21
	NT	NT	1.37	1.57	NT	1.34	NT
	NT	NT	1.41	1.65	NT	1.38	NT
76.2	0.76	0.95	1.21	1.28	1.10	1.22	1.49
	0.72	NT	1.31	1.31	1.10	1.38	1.27
	NT	NT	1.28	NT	1.07	1.41	NT
152.4	0.61	0.68	1.17	1.20	0.92*	1.20	1.08
	0.56*	0.64	1.08	1.26	0.99	1.15	1.01
	0.65	0.65	1.32*	1.36*	1.06	1.03	NT
304.8	0.56	0.63*	1.07*	0.92	0.75*	0.83	0.93
	0.58	0.54	0.99	0.91	0.85	0.92	0.88
	0.48*	0.63*	0.91	NT	0.89	0.85	NT

NT = specimens not tested.

* Values inconsistent with the trend of other tests.

Using Equation (2), the parameters B and d_0 (see Eqs. (2) and (4)) have been determined through linear regression analysis of the experimental data. The linear regression plot and the size-effect plot of the fit with the test data are shown in Figure (5).

The values obtained from the regression analysis for the parameter A and the fracture energy G_f are shown in Table (3). Values of $g_f(\alpha_0)$ were computed equal to 6.07 and 14.20 for relative notch length equal to 0.167 and 0.333, respectively. The Young's modulus of elasticity was computed from the formula of Carrasquillo, Nilson and Slate [13] $E = 3320 f_c'^{1/2} + 6900$ (MPa). As can be seen, only Series S1 and S2 do not comply entirely the standard requirements concerning about the limiting values of the coefficient of variation of the slope of the regression line (ω_A), the coefficient of variation of the intercept of the regression line (ω_C), and the relative width of scatter-band (m). According to RILEM TC89-FMT [28], the value of ω_A should not exceed 0.10 and the values of ω_C and m about 0.20. The values of ω_C for Series S2, and of ω_A for Series S1 are much higher than the recommended. Nevertheless, the values found for G_f cannot be considered inconsistent when compared with the results of the other tests.

Mixing the data from many different concretes, Bazant and Becq-Giraudon [3, 4] verified statistically the approximated ratio $G_F/G_f \approx 2.50$, with a coefficient of variation equal to 40%, which allows the calibration of the complete softening curve from the results obtained by the SEM. From the data of the present study it was obtained the ratio $G_F/G_f = 2.60$, with a coefficient of variation equal to 37.5%. Considering the data of Series S1, S2, S3, and S6 (same concrete mix) it was obtained the ratio $G_F/G_f = 2.88$, with a coefficient of variation equal to 38.1%. These values comply with the referred statistical study, given the uncertainty of the aforementioned ratio.

Table 3: Fracture energy obtained by the size effect method (adapted from Reference [16]).

Series	f_c' (MPa)	E (GPa)	a_0/d	$g_f(\alpha_0)$	A ($\mathrm{mm^{-1}Mpa^{-2}}$)	G_f (N/m)	ω_A	ω_C	m
S1	84	37.3	0.333	14.20	0.00659	57.70	0.196	0.204	0.222
S2	82	37.0	0.333	14.20	0.00979	39.23	0.138	0.361	0.213
S3	78	36.2	0.167	6.07	0.00220	76.13	0.100	0.081	0.116
S4	69	34.5	0.167	6.07	0.00285	61.71	0.076	0.119	0.118
S5	78	36.2	0.167	6.07	0.00212	78.81	0.109	0.068	0.092
S6	88	38.0	0.167	6.07	0.00293	54.41	0.086	0.116	0.191

5 Numerical simulation

Using the smeared approach, a numerical simulation was carried out for the three-point bend notched beam shown in Figure (6). The mesh was randomly generated using a quadratic isopara-

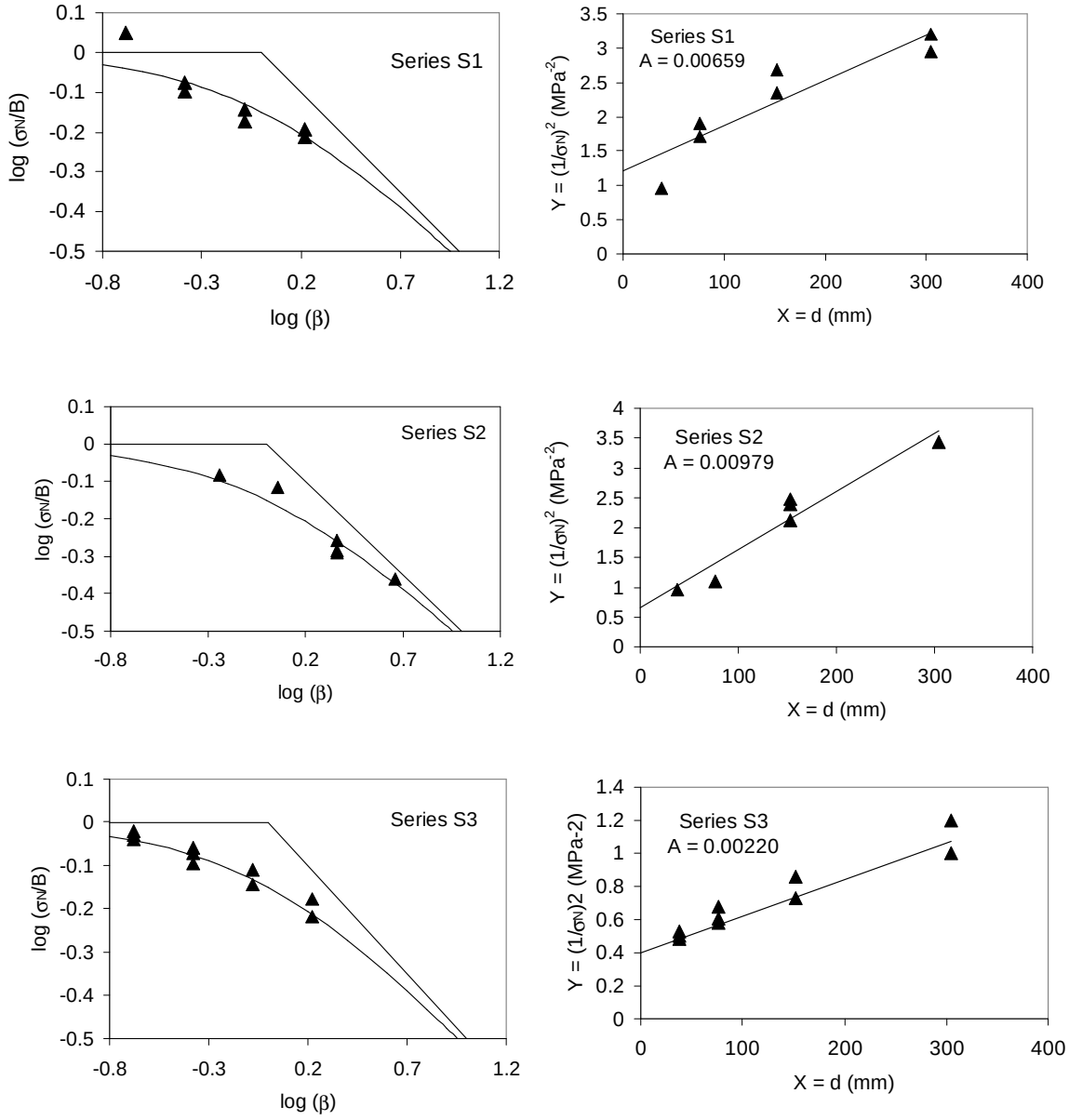

Figure 5: Size effect plot (left) and linear regression plot (right) constructed from experimental results (σ) obtained for Series S1 to S6.

metric triangular element (T6). The dimensions of the beam are 800x200 mm (length x height) with a notch of 20x50 mm (width x depth). The material parameters are: tensile strength f_t' = 3 MPa, fracture energy G_F = 75 N/m, modulus of elasticity E = 30000 MPa and Poisson's ratio ν = 0.2.

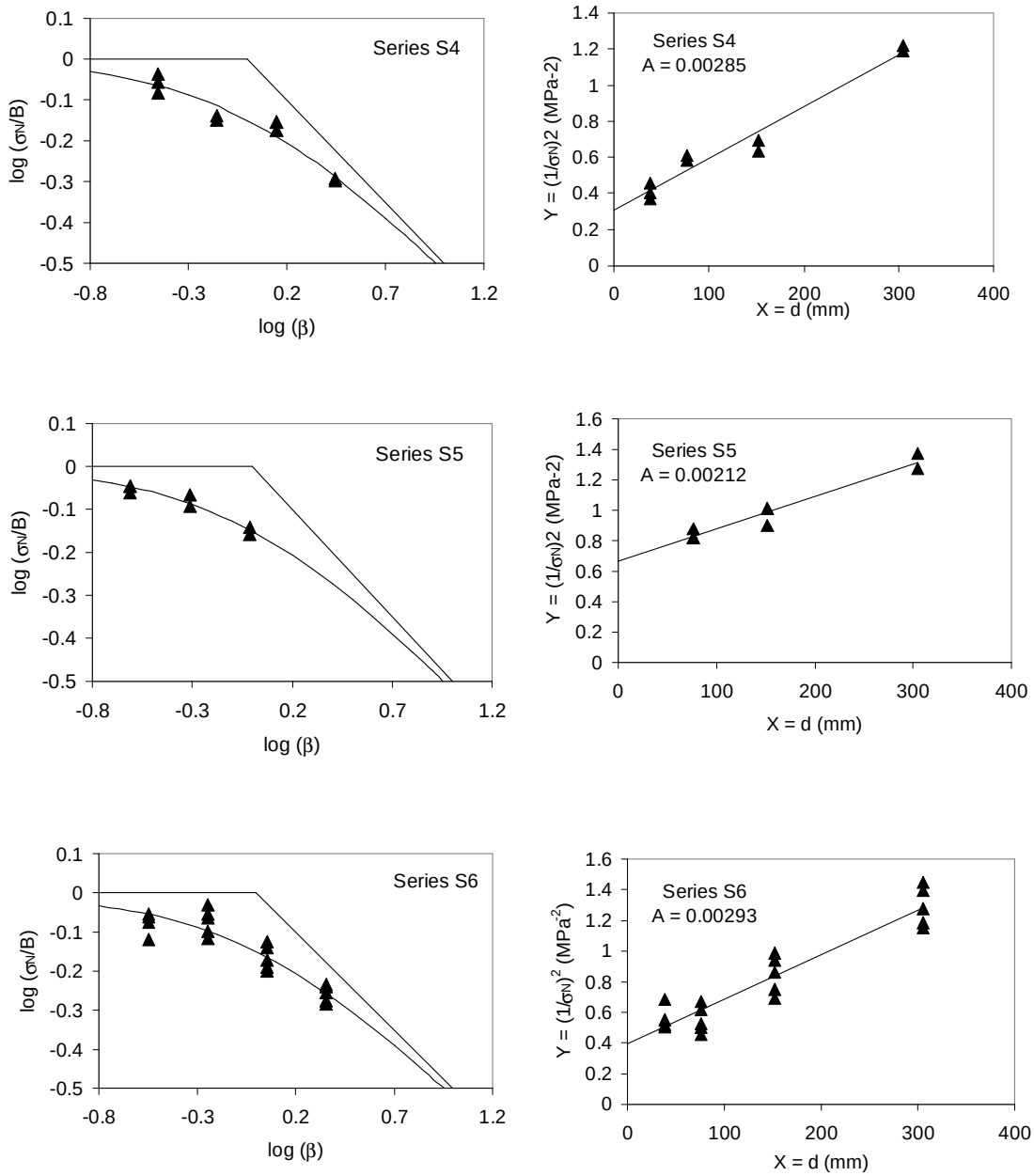

Figure 5: *(continued)* Size effect plot (left) and linear regression plot (right) constructed from experimental results (σ) obtained for Series S1 to S6.

The finite element analysis was performed using the program FEPARCS, developed by Elwi [17] at the University of Alberta, Canada. The energy-based plasticity model of Pramono and Willam [23] for plain concrete was used for the smeared analysis. This model has

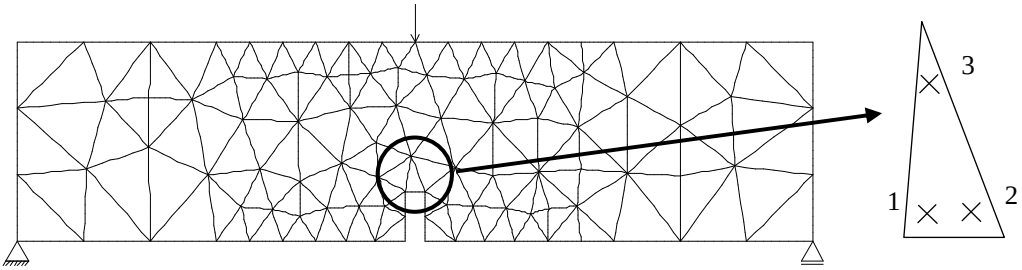

Figure 6: Finite element mesh for notched beam and Gauss points position for the circled element.

a unified formulation that covers the full load-response spectrum of the triaxial behavior of concrete in tension as well as in compression. The concrete behavior is modeled through a non-associated flow theory of plasticity, with hardening in the pre-peak regime and fracture-energy based softening in the post-peak regime. In this example, the degradation of the tensile strength was related to the crack opening displacement through the bilinear softening curve represented in Figure (7), which corresponds to the bilinear curve proposed by Petersson [22]. This curve has its kink point fixed at $w = 0.8G_F/f_t'$ and $\sigma = 1/3f_t'$ and the cohesive stress becomes zero for $w = 3.6G_F/f_t'$.

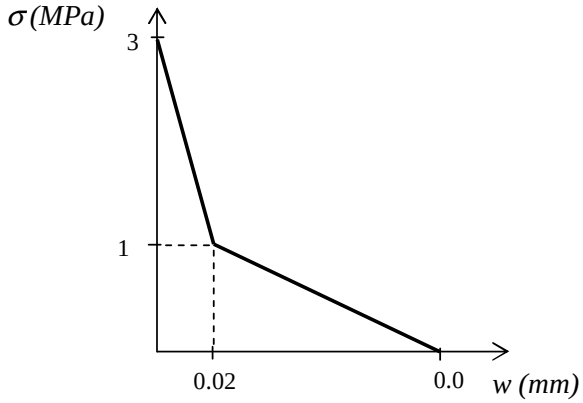

Figure 7: Bilinear softening curve considered in the numerical analysis.

The arc-length control was used to solve the system of equations. Due to highly localized failure mode, only some degrees-of-freedom that presented a high deformation gradient value had to be considered to compose the constraint equation [10]. Therefore, the indirect displacement control was activated as soon as the strain was localized in one or more elements. When the program identifies at least one Gauss point that shows a constitutive post-peak behavior, a flag is activated at the end of the step. On the next step, after the first interaction, all the elements that show softening are selected and define a plastic region. The degrees-of-freedom inside this

region are then used for indirect displacement control during the equilibrium interactions. This procedure was repeated in the subsequent steps. The deformed configuration (amplified by a factor of 1000) and the stress configuration related to the maximum principal stress σ_1 at peak load are shown in Figure (8). The stress concentration at the finite element close to the notch is evident in the figure.

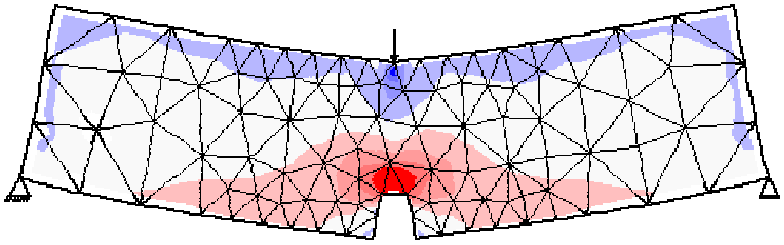

Figure 8: Deformed (x1000) and stress configurations at peak load.

The load-deflection curve of the upper-center of the beam, obtained in the analysis, is presented in Figure (9). The softening stresses were analyzed for the finite element where the strain localization initially occurs. This element is shown in detail in Figure (6). The stresses were computed for the Gauss points 1, 2 and 3, for the loads corresponding to points A, B, C, D, E and F in the curve.

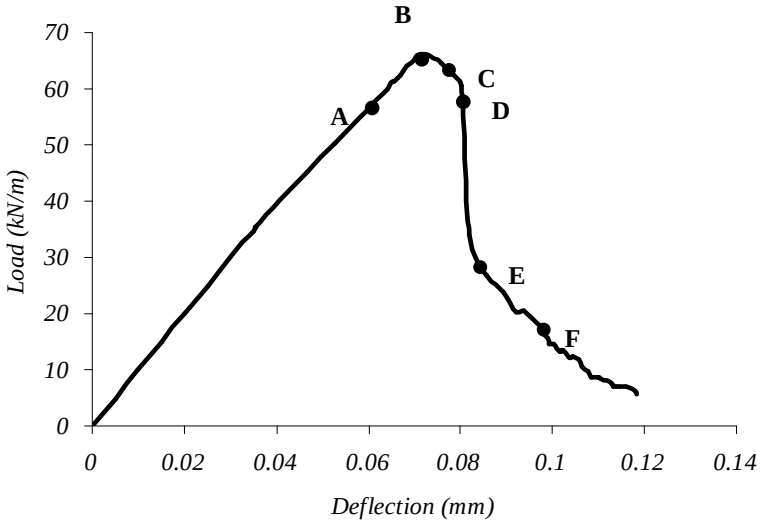

Figure 9: Load-deflection of the upper-center of the beam.

The results, in terms of the cohesion parameter given by the ratio $\sigma_t/f_t^{'}$ (softening stress/ tensile strength), are presented in Table (4). For the Gauss point 1 its possible to see that the softening stress is reduced to 75% of the tensile strength in point B at the peak load.

Consequently, at maximum load, the cohesive crack will never be opened enough for the tail stresses of the softening curve to occur. The strain localization follows the path of the Gauss points 1 and 3, but only for point E there is a significant reduction of the cohesive stress. Consequently, not only the ascending part of the curve, but also a considerably part of the descending branch of the load-deflection curve can be obtained with the application of the linear softening diagram corresponding to the fracture energy G_f.

Table 4: Cohesion parameters given by the ratio softening stress/tensile strength.

Gauss Points	$\sigma_t / f_t^{'}$					
	Points in the load-deflection curve					
	A	B	C	D	E	F
1	1.00	0.75	0.69	0.62	0.28	0.11
2	1.00	1.00	1.00	1.00	1.00	1.00
3	1.00	1.00	1.00	1.00	0.45	0.23

6 Conclusions

Three-point bend notched beams were tested at the Technological Institute at PUC-Rio (ITUC) in order to study the fracture properties of HPC. The fracture energy was measured by the WFM and by the SEM, which allowed establishing a relationship between the results obtained by the two processes.

The SEM has the advantage of providing fracture parameters that are size and shape independent, with a lower scatter of results in comparison with the work-of-fracture method [3]. Another advantage is that the experiments are feasible with no need of a servocontrolled testing equipment, since only the peak loads are necessary to be determined, and not the complete load-deflection curve. As shown in the present work, only the initial part of the softening curve, which corresponds to the fracture energy G_f determined by the SEM, is necessary to determine the peak load when performing numerical analysis for normal-sized structures. For structures of larger dimensions, however, the cohesive stress that corresponds to the maximum load will be lower than the elbow of the softening curve, according to Guinea et al. [18]. In this case, the complete stress-separation curve must be provided in the analysis. The complete load-deflection curve is also required most of the times for commercial programs, applied to concrete constitutive models when performing finite element analysis. Therefore, for practical purposes, it would be of interest to establish a correlation between the fracture energy obtained by the two processes. The main conclusions that can be drawn from this study are the following:

- The ratio G_F/G_f between the fracture energy measured by the work-of-fracture method

and the size effect method was found equal to 2.60 considering all the specimens, and 2.88 for the specimens cast with the same type of concrete, with a coefficient of variation equal to 37.5% and 38.1%, respectively. These values comply with the statistical study carried out by Bazant and Becq-Giraudon [3, 4].

- The numerical simulation presented in this paper shows that the cohesive stress is reduced to only 75% of $f_t^{'}$ at the peak load. For normal-sized structures, one can conclude that the numerical model will provide the same maximum load if the cohesive model is replaced by a straight line corresponding to the initial tangent of the softening stress-separation curve. For larger structures, the application of the linear softening curve should be evaluated according to the procedure presented in the work of Guinea et al. [18].

References

[1] RILEM 50-FMC. Determination of the fracture energy of mortar and concrete by means of three-point load tests on notched beams. *RILEM Draft Recommendation*, 18(106):285–290, 1985.

[2] T.L. Anderson. *Fracture Mechanics - Fundamentals and Applications.* CRC Press, Boca Raton - Florida - USA, 1991.

[3] Z.P. Bazant and E. Becq-Giraudon. Estimation of fracture energy from basic characteristics of concrete. In R. de Borst, J. Mazars, G. Pijaudier-Cabot, and J.G.M. van Mier, editors, *Fracture Mechanics of Concrete Structures*, pages 491–495, Paris, 2001. Balkema Publishers.

[4] Z.P. Bazant and E. Becq-Giraudon. Statistical prediction of fracture parameters of concrete and implications for choice of testing standard. *Cement and Concrete Research*, 32(4):529–556, 2002.

[5] Z.P. Bazant, J.K. Kim, and P.A. Pfeiffer. Nonlinear fracture properties from size effect tests. *Journal of Structural Engineering*, 112:289–387, 1986.

[6] Z.P. Bazant and B.H. Oh. Crack band theory for fracture of concrete. *Materials and Structures*, 16:155–177, 1983.

[7] Z.P. Bazant and P.A. Pfeiffer. Determination of fracture energy from size effect and brittleness number. *ACI Materials Journal*, 84:463–480, 1987.

[8] Z.P. Bazant and J. Planas. *Fracture and Size Effect in Concrete and Other Quasibrittle Materials.* CRC Press, Boca Raton - Florida - USA, 1998.

[9] Z.P. Bazant, Q. Yu, and G. Zi. Choice of standard fracture test for concrete and its statistical evaluation. *International Journal of Fracture*, 118:303–337, 2002.

[10] R. De Borst. *Non-linear analysis of frictional materials.* PhD thesis, Delft University, Netherlands, 1986.

[11] V.S. Caland. Experimental results of fracture parameters for high-performance concrete. Master's thesis, Department of Civil Engineering - PUC-Rio, Rio de Janeiro - Brazil, 2001.

[12] A. Carpinteri. Cracking of strain-softening materials. *Static and Dynamics Fracture Mechanics*, pages 311–365, 1994.

[13] R.L. Carrasquillo, A.H. Nilson, and F.O. Slate. Properties of high strength concrete subject to short-term loads. *ACI Journal*, 78(3):171–178, 1981.

[14] CEB-FIP Model Code 1990 – final draft. Bulletin d'Information du Comité Euro-International du Béton, 1991.

[15] D. Darwin, S. Abraham, R. Kosul, and S.G. Luan. Fracture energy of high-strength concrete. *ACI Materials Journal*, 98(5):410–417, 2001.

[16] R.A. Einsfeld and M.S.L. Velasco. Fracture parameters for high-performance concrete. *Cement and Concrete Research*, 36(3):576–583, 2006.

[17] A.E. Elwi. *FEPARCS 92 - A Description and User's Manual*. Department of Civil Engineering - University of Alberta, 1992.

[18] G.V. Guinea, J. Planas, and M. Elices. Correlation between the softening and the size effect curves. In H. Mihashi, H. Okamura, and Z.P. Bazant, editors, *Size Effect in Concrete Structures*, pages 233–244, London, 1994. E&FN Spon.

[19] G.V. Guinea, J. Planas, and M. Elices. A general bilinear fit for the softening curve of concrete. *Materials and Structures*, 27:99–105, 1994.

[20] A. Hillerborg. The theoretical basis of a method to determine the fracture energy g_F of concrete. *Materials and Structures*, 18(106):291–296, 1985.

[21] A. Hillerborg, M. Modéer, and P.E. Petersson. Analysis of crack formation and crack growth in concrete by means of fracture mechanics and finite elements. *Cement and Concrete Research*, 6:773–782, 1976.

[22] P.E. Petersson. Crack growth and development of fracture zone in plain concrete and similar materials. Technical Report TVBM-1006, Division of Building Materials - Lund Institute of Technology, Lund - Sweden, 1981.

[23] E. Pramono and K. Willam. Fracture energy-based plasticity formulation of plain concrete. *Journal of Engineering Mechanics*, 115(6):1183–1204, 1989.

[24] G.A. Rao and B.K.R. Prasad. Fracture energy and softening behavior of high-strength concrete. *Cement and Concrete Research*, 32(2):247–252, 2002.

[25] P.E. Roelfstra and F.H. Wittmann. Numerical methods to link strain softening with failure of concrete. In F.H. Wittmann, editor, *Fracture Toughness and Fracture Energy of Concrete*, pages 163–175, Amsterdam, 1986. Elsevier Science.

[26] K. Rokugo, M. Iwasa, T. Suzuki, and W. Koyanagi. Testing methods to determine tensile strain softening curve and fracture energy of concrete. In H. Mihashi, H. Takahashi, and F.H. Wittmann, editors, *In Fracture Toughness and Fracture Energy: Test Methods for Concrete and Rock*, pages 153–163, Rotterdam, 1989. Balkema.

[27] M.L.O. Silva. Experimental study on fracture energy and size-effect of high-performance concrete. Master's thesis, Department of Civil Engineering - PUC-Rio, Rio de Janeiro - Brazil, 2000.

[28] RILEM TC89-FMT. Size effect method for determining fracture energy and process zone size of concrete. *Materials and Structures*, 23:461–465, 1990.